BBA 75699

ON THE LOCATION OF 1-ANILINO-8-NAPHTHALENE-SULFONATE IN LIPID MODEL SYSTEMS

AN X-RAY DIFFRACTION STUDY

W. LESSLAUER, J. CAIN AND J. K. BLASIE

Johnson Research Foundation, University of Pennsylvania, Philadelphia, Pa. (U.S.A.)

(Received March 29th, 1971)

SUMMARY

The electron density distribution across the magnesium stearate bimolecular leaflet is calculated from the relative intensities of discrete X-ray diffraction patterns from magnesium stearate multilayers. The generalized Patterson function $P'(x)$ is calculated for a system with 3 unit cells. The autocorrelation function $P_0(x)$ is determined from $P'(x)$. The electron density distribution $\mu(x)$ is calculated by a deconvolution of $P_0(x)$ through a recursion process.

Diffraction is recorded also from magnesium stearate multilayers with large numbers of unit cells. Phase angles are determined from $\mu(x)$ and by swelling experiments. Electron density distributions $\rho(x)$ are calculated by Fourier syntheses. 1-Anilino-8-naphthalene-sulfonate (ANS) is incorporated into this system and the effects on its structure are discussed.

X-ray diffraction data from lecithin/cardiolipin dispersions are presented. These diffracted intensities are a continuous function of the diffraction angle; they can be considered to arise from randomly oriented single bimolecular leaflets. The generalized Patterson function $P'(x)$ is calculated and it is shown that in this case $P'(x)$ is identical to the autocorrelation function $P_0(x)$. $\mu(x)$ is calculated by a deconvolution of $P_0(x)$. ANS in different concentrations is incorporated in the lecithin/cardiolipin bimolecular leaflet and the resulting perturbation of its structure is discussed.

INTRODUCTION

Fluorescent molecules like 1-anilino-8-naphthalene-sulfonate (ANS) have been used as probes for structural studies of protein molecules (*e.g.* ref. 1) and biological membranes. These dyes are valuable because the fluorescence characteristics are sensitive to their local environment. For a detailed analysis of the fluorescence response of ANS in a given membrane, however, the structure of the membrane and the location of the probe in it should be known. Such knowledge may provide some insight into the function of the membrane, since it was shown that the fluorescence of ANS can depend on the functional state of a biological membrane[2,3].

ANS is known to bind to nonpolar regions of protein molecules such as the

Abbreviation: ANS, 5-anilino-8-naphthalene-sulfonate.

heme binding site of apomyoglobin[1]. Biological membranes contain a variety of proteins and lipids. It is generally thought that the lipids in biological membranes aggregate in such a way as to form lipid hydrocarbon cores. ANS may be expected to bind to such hydrocarbon cores, if they are part of the structure of a biological membrane[4,5].

Lipid hydrocarbon cores exist in model systems where polar lipid molecules are arranged in bimolecular leaflets. Discrete diffraction was obtained from magnesium stearate multilayers and the electron density distribution across the bimolecular leaflet was calculated. In addition, the continuous diffraction from dispersions of single layered phospholipid vesicles was recorded, and the electron density distribution across the phospholipid bimolecular leaflet was obtained.

ANS was incorporated in both model systems and the effects on the structure of the bimolecular leaflets are discussed.

Some of the results reported have been presented briefly elsewhere[6].

MATERIALS AND METHODS

Stearic acid with a purity of better than 99% was purchased from Applied Science Laboratory. Purified cardiolipin was purchased from Sylvana Co. Synthetic dipalmitoyllecithin was obtained from Calbiochem; this preparation contained a small amount of free fatty acid which could be detected by thin layer chromatography. These substances were used without further purification. All other reagents were of analytical grade. Organic solvents were redistilled before use. ANS was obtained as sodium salt from Eastman Kodak and purified after the procedure of WEBER AND YOUNG[7]. It was stored as a 0.3 M solution in ethanol in the dark at 0°. The stock solution was faintly yellow.

Magnesium stearate multilayers were built up on a curved glass slide with a radius of 20 mm coated with a freshly evaporated silver mirror after the method of BLODGETT[8]. The glass slide was dipped mechanically through a monomolecular stearic acid film on the surface of a 10^{-3} M $MgCl_2$ solution (pH 7.5) in a Langmuir trough until the desired number of bimolecular leaflets was built up. The film in the Langmuir trough was kept continuously near the collapse pressure by a moving float[9].

Dispersions of phospholipid vesicles were prepared with lecithin and cardiolipin in a molar ratio of 8:1 in the following way[10,11]: Small amounts of phospholipids were dried down from organic phase on the wall of a glass vessel and subsequently suspended in a 0.015 M phosphate buffer (pH 7.5). The suspensions were made as concentrated as possible (5–7%, w/v). They were then sonicated at 0° until they were optically clear. There was no indication that this procedure resulted in a nonhomogeneous vesicle population because of separation of lecithin and cardiolipin. The sample was finally transferred to a cell made from polymethacrylate with Melinex windows for X-ray diffraction experiments. The pathlength of X-rays in the sample cell was 1.5 mm. Multilayer specimens were kept in a closed chamber with Melinex windows which could be flushed with helium gas of defined relative humidity. 0% relative humidity was obtained by placing the specimen over P_2O_5 in the camera vacuum at about 10^{-2} torr (vacuum dried specimen). Experiments were done at room temperature (28 ± 2°).

A Jarrell-Ash microfocus X-ray unit with a focusing cathode was the radiation

source. Ni-filtered Cu–K α-radiation was used. The effective focal area on the anode was 1.4 mm $\times$ 5 μm. The camera axis was set at an angle of 5° with the anode surface. X-ray cameras were of the Franks' type[12] and were equipped with vacuum paths. The line source of X-rays was used to obtain the diffraction patterns. The beam width at the guard slit was of the order of 150 μm. The half-width of the beam at the film was 125 μm. For multilayer and dispersion specimens the height of the beam at the guard slit was 2 mm.

Diffraction patterns were recorded on Ilford Industrial G X-ray film employing cylindrical cassettes with diameters of 62.5 or 125 mm. Densitometer tracings of the films were done with a Joyce, Loebl Mark III CS microdensitometer. The integrated intensities for discrete diffraction patterns from stearate multilayers with many unit cells were obtained from the product of the half-width and the peak maximum on the densitometer tracing. The correction factor for the lamellar reflection of order h for the integrated intensities was h^2. The intensities for discrete diffraction patterns from magnesium stearate multilayers with a small number of unit cells or from phospholipid dispersions were obtained as a function of the reciprocal space co-ordinate $x^* = (2 \sin \theta)/\lambda$ from densitometer tracings. The step increase in x^* was $0.52 \cdot 10^{-3}$ Å^{-1}.

The background for the dispersions was determined by the assumption that

TABLE I

INTENSITY DATA FOR MAGNESIUM STEARATE MULTILAYERS WITH AND WITHOUT ANS

The values for I_{obs} (h) for N = 25 and 43 are the integrated intensities of the lamellar reflections; for N = 3, the maximum amplitude of the reflections in the densitometer tracings are given. $\Delta/(1/D)$ is the half-width of the reflections in units of $1/D$. Intensities are normalized to $\sum_h I_{obs}(h)$ = 1.0. Signal-to-noise ratio is the ratio of the amplitudes of signal and noise of the strongest reflections observed.

h	*Magnesium stearate*						*Magnesium stearate + ANS*					
	Hydrated				*Vacuum dried*		*Hydrated*				*Vacuum dried*	
	$N = 3$		$N = 43$		$N = 43$		$N = 3$		$N = 25$		$N = 25$	
	I_{obs}	$\frac{\Delta}{1/D}$	I_{obs}	$\frac{\Delta}{1/D}$	I_{obs}	$\frac{\Delta}{1/D}$	I_{obs}	$\frac{\Delta}{1/D}$	I_{obs}	$\frac{\Delta}{1/D}$	I_{obs}	$\frac{\Delta}{1/D}$
1	0.544	(0.240)	0.507	0.090	0.398	0.090	0.674	(0.240)	0.675	0.092	0.527	0.070
2	0.152	0.241	0.124	0.095	0.084	0.075	0.128	0.240	0.114	0.081	0.079	0.070
3	0.258	0.241	0.276	0.095	0.362	0.100	0.170	0.240	0.178	0.097	0.281	0.075
4	0.009	0.254	0.003	0.090	0.026	0.085	0.005	0.240	0.004	0.103	0.018	0.075
5	0.030	0.254	0.024	0.101	0.104	0.100	0.015	0.240	0.011	0.092	0.078	0.085
6	0.008	0.268	0.020	0.106	0.004	0.100	0.008	0.240	0.007	0.092	0.002	0.090
7			0.002	0.122	0.020	0.100			~0.001	0.092	0.012	0.090
8			0.026	0.116	0				0.007	0.108	0	
9			0.006	0.127	0.002	0.150			~0.001	0.087	0.002	0.135
10			0.010	0.122					0.002	0.108		
11			?	?								
12			0.003	0.180								
Signal-to-noise ratio	60		240		310		58		430		300	

the intensity minima between the diffraction maxima are zero and a smooth curve was fitted through the minima of the intensity curve whose form was characteristic for the camera. The correction factors for the intensity were $(x^*)^2$ for phospholipid

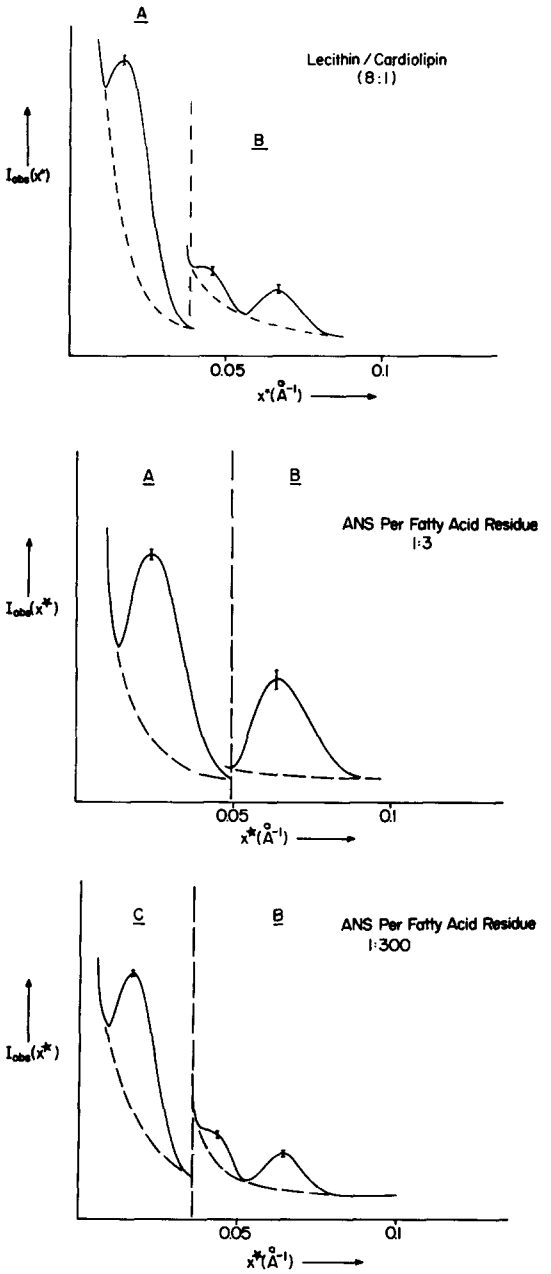

Fig. 1. Observed diffracted intensities $I_{obs}(x^*)$ as a function of $x^* = 2 \sin\theta/\lambda$ ($Å^{-1}$) from dispersions of dipalmitoyllecithin/cardiolipin (1A) and dipalmitoyllecithin/cardiolipin with ANS in high (1B) and low (1C) concentration. Noise in the densitometer tracing is indicated for each maximum as peak to peak noise. For optical wedges *A*, *B*, *C* and scaling factors see text.

dispersions and x^* for magnesium stearate multilayers with a small number of unit cells. No correction for slit smearing was necessary. Signal-to-noise ratios are given in Table I for the strongest reflections. The noise level in the densitometer tracings for phospholipid dispersions is given as peak to peak noise in Fig. 1. Unit cell dimensions from discrete diffraction patterns were calculated from Bragg's equation ($n\lambda = 2D \sin\theta$).

Fluorescence emission was recorded on a Hitachi Fluorescence Spectrophotometer.

Computations were performed on a PDP 6 computer of the Medical School of the University of Pennsylvania.

RESULTS

Magnesium stearate multilayers

Multilayers of magnesium stearate with a varying number, N, of bimolecular layers, or unit cells, were built up. Freshly made specimens or specimens kept in a saturated water vapor atmosphere appeared as a turbid film on the silver surface. After vacuum drying the same specimen showed the multilayers as a highly transparent film, exhibiting, depending on the number of layers, interference colors of the kind observed with barium stearate multilayers[8].

The reflections in X-ray diffraction patterns arising from the electron density distribution along an x-axis normal to the plane of the bimolecular leaflet ("lamellar reflections") were different for specimens kept at 100 % relative humidity during the exposure ("hydrated specimens") and for vacuum dried specimens. In hydrated specimens the unit cell dimension D along the x-axis was 51.0 ± 0.6 Å (for a specimen with $N = 43$) as compared to 48.3 ± 0.6 Å for the same specimen after vacuum drying. The reproducibility for D for independent specimens was well within the limits given. A marked difference in the relative integrated intensities of the lamellar reflections was observed in diffraction patterns from hydrated and vacuum dried specimens (Table I). The 4th and 7th lamellar reflection from hydrated multilayers are very weak compared to the neighboring reflections, and the 8th reflection is relatively strong. In diffraction patterns from vacuum dried specimens, the 6th reflection was weak and the 8th was missing. The 4th and 7th reflections were, in contrast to the hydrated case, strong. Up to 12 reflections were observed from hydrated magnesium stearate multilayers and up to 9 from vacuum dried specimens. The reproducibility of the integrated intensity of the lamellar reflections was studied by comparing the reflections from two independent specimens. For this comparison the integrated intensities were normalized to the sum of the intensities of all reflections of the diffraction pattern. For hydrated magnesium stearate the deviations were less than ± 6 % for reflections stronger than 0.006 on the intensity scale of Table I and less than ± 25 % for the weaker reflections. The variation in the Patterson function $P(x)$

$$P(x) = \frac{2}{D} \sum_h |F(h)|^2 \cdot \exp(-2\pi i x h/D) \qquad (1)$$

where

$$h^2 \cdot I_{obs}(h) \propto |F(h)|^2$$

($I_{obs}(h)$ = observed diffracted intensity) for the two sets of intensity data for any x was less than $\pm$ 2 % of the peak at the origin. For vacuum dried magnesium stearate, the deviations were less than $\pm$ 12 % for reflections stronger than 0.011 in Table I and less than $\pm$ 25 % for weaker reflections. The variation in $P(x)$ for the two sets of intensity data for any x was less than $\pm$ 7 % of the peak at the origin.

Six lamellar reflections were observed from a hydrated specimen with 3 unit cells of magnesium stearate. Larger deviations of the peak maxima from the ideal reciprocal lattice points h/D were observed than with specimens with many unit cells, especially for the 4th reflection. The value for D was 51.6 $\pm$ 0.8 Å. The value for the intensity given in Table I for this case is the maximum amplitude of the respective reflection in the densitometer tracing. The half-width of the reflections is larger by a factor of $\sim$ 2.5 than for the specimens with many unit cells (Table I). The half-width of the primary beam at the film in units of $1/D$ with D = 50.0 Å was 0.0325.

Magnesium stearate multilayers with incorporated ANS

Magnesium stearate multilayers which contained ANS were built up in the following way. Stearic acid and ANS in a molar ratio of 1 ANS per 5 fatty acid molecules were dissolved in hexane with a small amount of added ethanol. Monomolecular films of this mixture were spread on the surface of a 10^{-3} M $MgCl_2$ solution (pH 7.5) in the Langmuir trough. This mixed monomolecular film was then transferred onto a silver mirror in the same way as with pure fatty acid films. In a specimen with 25 bimolecular leaflets, the fluorescence of ANS could be easily observed in the spectrophotometer. Multilayers of magnesium stearate and ANS showed the same difference in optical appearance between hydrated and vacuum dried specimens as the magnesium stearate multilayers without ANS.

In the specimen with incorporated ANS (N = 25) the unit cell dimensions D were 52.2 $\pm$ 0.3 Å and 48.4 $\pm$ 0.6 Å for the hydrated and the vacuum dried cases, respectively. The reproducibility of D for independent specimens was within the limits given. There were no large differences in the relative intensities of the lamellar reflections due to the presence of ANS in the magnesium stearate bimolecular leaflet in either the hydrated or the vacuum dried case. With hydrated specimens the 4th and especially the 7th reflection was weak and the 8th reflection strong. With vacuum dried specimens, the 6th reflection was weak, the 8th reflection was missing and the 4th and 7th reflections were strong (Table I). Up to 10 reflections were observed with hydrated specimens and up to 9 reflections with vacuum dried specimens of ANS/magnesium stearate multilayers. The deviations in the integrated intensities for two independent specimens were for the hydrated specimens less than $\pm$ 6 % for reflections stronger than 0.007 in Table I and less than $\pm$ 50 % for weaker reflections. The resulting variation in $P(x)$ for any x was less than $\pm$ 5 % of the peak at the origin. The deviations in the vacuum dried specimens were less than $\pm$ 10 % for reflections stronger than 0.060 in Table I and less than 30 % for weaker reflections. The variation in $P(x)$ for any x was less than $\pm$ 7 % of the peak at the origin.

Diffraction was recorded also from hydrated specimens with 3 bimolecular leaflets of magnesium stearate with incorporated ANS in the same ratio as above. Peak maxima and half-width of the first 6 reflections for such a specimen are given in Table I. The unit cell dimension for this specimen is 51.4 $\pm$ 1.0 Å.

Phospholipid dispersions

X-ray diffraction was recorded from a sonicated dipalmitoyllecithin/cardiolipin dispersion in a molar ratio of 8:1. The diffracted intensity was a continuous function of the diffraction angle. No discrete reflections were observed. The microdensitometer tracing is given in Fig. 1A. Three broad maxima can be distinguished. *A* and *B* refer to optical wedges of 3.0 and 0.85 absorbance, respectively. The ratio of the scaled but uncorrected first and third maxima is 32.5. Peak to peak noise is indicated for each maximum. The intensity was recorded to a diffraction angle corresponding to spacings of 12.7 Å. For subtraction of background see MATERIALS AND METHODS.

Phospholipid dispersions with incorporated ANS

Dispersions of mixed lecithin/cardiolipin (8:1) and ANS were prepared in an analogous way to the pure phospholipid dispersion. ANS was dissolved in ethanol and added to the phospholipids before they were dried down from organic phase. Densitometer tracings of diffraction patterns from lecithin/cardiolipin dispersions with ANS in concentrations of 1 mole ANS per 3 moles of fatty acid residues and of 1 mole ANS per 300 moles of fatty acid residues of the phospholipid mixture are shown in Figs. 1B and 1C. As in patterns from the pure phospholipid dispersions, the diffracted intensities were a continuous function of the diffraction angle and no discrete reflections were observed. Diffracted intensities extended out to a diffraction angle corresponding to spacings of 12.3 Å and 12.7 Å for the preparations with high and low ANS concentrations, respectively. Although this was approximately the same Bragg angle to which diffraction from the pure phospholipid dispersion was observed, only 2 maxima could be observed in the preparation with the high ANS concentration. These maxima are broader than those of the reference experiments. With the lower ANS concentration 3 maxima are observed, but the second maximum is weaker than in the reference pattern.

B and *C* in Fig. 1B (low ANS concentration) refer to optical wedges of 0.38 and 1.76 absorbance, respectively. The ratio of the scaled but uncorrected first and third maxima is 45.4. *A* and *B* in Fig. 1C (high ANS concentration) refer to optical wedges of 3.0 and 0.38 absorbance, respectively. The ratio of the scaled but uncorrected first and second maxima is 13.2.

DISCUSSION

Both model systems used in the experiments described above present in principle the structure of the bimolecular lipid leaflet. In this arrangement two monomolecular films of lipid molecules with opposite orientation face each other so that a mirror plane exists between the two monomolecular films. The following discussion is based on this symmetry of the one dimensional unit cell along the x-axis normal to the plane of the bimolecular leaflet. Only diffraction arising from the electron density distribution along the x-axis will be considered in the discussion. With oriented multilayer specimens diffraction whose origin lies in electron density contrast in the plane of the bimolecular leaflet can be recognized in the pattern and therefore be neglected. Phospholipid dispersions can be regarded as systems composed of randomly oriented plane single bimolecular leaflets (see APPENDIX). Contributions to the diffracted intensities from the electron density distribution along the x-axis and in the

plane of the bimolecular leaflet cannot in general be distinguished. The maximum diffraction angle, however, to which intensities were recorded in the dispersion patterns, corresponds to spacings of 12–13 Å. At this resolution, the structure of the unit cell can be considered to have uniform electron density in the plane of the leaflet, since the separation of the fatty acid chains or the phosphate groups certainly is smaller than 10 Å. The diffracted intensities then arise only from the variation in electron density along the x-axis.

Magnesium stearate multilayers

The change in optical appearance upon vacuum drying a hydrated magnesium stearate multilayer specimen and the linked decrease in the dimension of the unit cell observed in X-ray diffraction experiments indicate that there are water spaces in these systems. Multilayers from barium stearate do not take up water, and diffraction patterns from hydrated and vacuum dried specimens are identical.

The electron density distribution of the barium stearate bimolecular leaflet has been established previously using 17 lamellar reflections[13]; it contains two peaks of high relative electron density which can only be due to a relatively heavy atom. The Patterson functions for the hydrated and vacuum dried magnesium stearate structure also show that narrow regions of high relative electron density exist in the unit cell. This and the difference in the swelling behavior of the multilayer specimen, depending on whether $BaCl_2$ or $MgCl_2$ solutions (pH 7.5) are used in the Langmuir trough during the process of building up the multilayer specimen, are evidence that Mg^{2+} (or Ba^{2+}) are incorporated as counterions of the carboxyl groups into the multilayer structure.

The width of the lamellar reflections from the hydrated magnesium stearate multilayer specimen with 3 unit cells (Table I) may be regarded with good approximation as the true width of the maxima of the interference function. The half-width of the peaks is much larger than that for a specimen with many unit cells and is nearly the same for all reflections (Table I). A generalized form of the Patterson function $P'(x)$ may then be calculated by an integral Fourier transformation of the intensity data[13]. $P'(x)$ then takes into account information contained in the shape of the reflections and shifts of the peak maxima from the ideal reciprocal lattice points[14].

$$P'(x) = \int_{-\infty}^{\infty} |F(x^*)|^2 \cdot \exp(-2\pi i x \cdot x^*)\, \mathrm{d}x^* \qquad (2)$$

In this case, $|F(x^*)|^2$ is proportional to $x^* \cdot I_{obs}(x^*)$. The correction factor x^* arises from the geometry of the specimen. Since the primary beam can be treated approximately as a δ-function, no correction for beam divergence is needed. $P'(x)$ is shown in Fig. 3.

As has to be demanded $P'(x)$ disappears rapidly outside $\pm N \cdot D$, where $N = 3$ is the number of unit cells. A peak around $\pm 4 \cdot D$ can still be observed; its amplitude, however, has decreased to 5 % of $P'(0)$. Under these conditions, the Patterson function of a single unit cell $P_0(x)$ can be calculated from $P'(x)$ (see APPENDIX). $P_0(x)$ is the autocorrelation function of the structure and it can be deconvoluted according to HOSEMANN AND BAGCHI[14], since the structure has a center of symmetry. The deconvolution is performed by a recursion process (ref. 14, p. 122–131) and the electron

density distribution $\mu(x)$ obtained in this way for the hydrated magnesium stearate bimolecular leaflet is shown in Fig. 4; peaks of high relative electron density near $\pm D/2$ are separated by a region of low and nearly constant electron density with a central trough. $\mu(x)$ establishes that the hydrocarbon interior of the stearate bimolecular leaflet in the hydrated magnesium stearate multilayer is analogous to that of the barium stearate structure established previously[13]. Computed values and an average symmetric curve for $\mu(x)$ are given in Fig. 4. The asymmetries in the computed $\mu(x)$ are due to computation artefacts and to the choice of a value for D. The

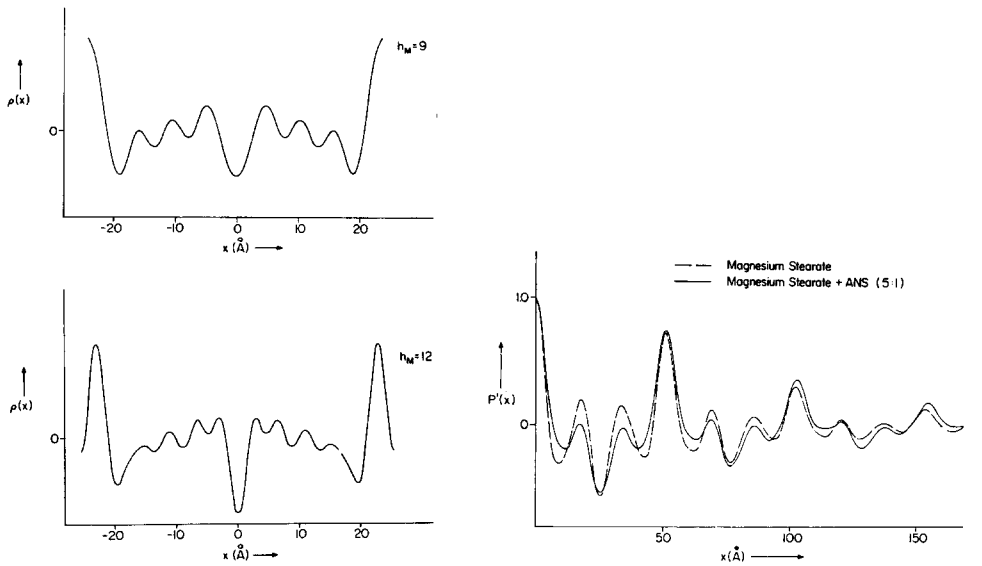

Fig. 2. Profile of the relative electron density $\rho(x)$ (in arbitrary units) of the unit cell of the magnesium stearate bimolecular leaflet in the vacuum dried (top) and hydrated (bottom) state. h_M designates the maximum number of reflections used in the Fourier synthesis. For correction factors and normalization see text.

Fig. 3. Generalized Patterson function $P'(x)$ for structures with 3 magnesium stearate bimolecular leaflets in the hydrated state with (———) and without (– – – –) incorporated ANS. Normalization is for $P'(0) = 1.0$. For correction factors see text.

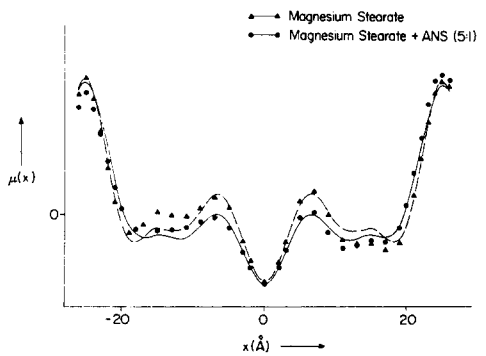

Fig. 4. Profile of the relative electron density $\mu(x)$ (in arbitrary units) for the hydrated magnesium stearate bimolecular leaflet with (———) and without (– – – –) incorporated ANS, as obtained by deconvoluting $P_0(x)$. Average symmetric curves are drawn; ▲ and ● mark the computed values for magnesium stearate and ANS/magnesium stearate, respectively (see text).

values for different $\mu(x)$ vary systematically around the same symmetric curve, if μ-functions are calculated with systematically increasing values for D within the limits imposed by the variation of the sampling intervals h/D. To choose an average $\mu(x)$ symmetric around the origin, therefore, is justified.

It was shown previously[13] that the barium stearate bimolecular leaflet can be described to a good approximation by the following model for the electron density distribution $\rho(x)$

$$\rho(x) = g(x^*)\{A\cdot\delta(x + D/2) + A\cdot\delta(x - D/2) - B\cdot\delta(x)\} \quad (3)$$

($g(x)$ = Gaussian function; $\delta(x)$ = Dirac delta function; * stands for convolution operation; A,B = constants, with $A > B$). This model shows peaks of high relative electron density at $\pm D/2$ corresponding to the layer of Ba^{2+} and a trough in the center of the unit cell in the region of the terminal methyl groups of the fatty acid chains. The electron density in the region of the methylene groups of the fatty acid chains in the model is assumed to be identical with the average electron density. The structure factor $F(x^*)$ is then

$$F(x^*) = G(x^*)\cdot\{2A\cos(2\pi\cdot x^*\cdot D/2) - B\} \quad (4)$$

The proper set of phase angles φ_h for such a structure is an alternating sequence of π and 0 for the lamellar reflections of order $h = 1,2,3\ldots$. The odd order lamellar reflections will be systematically more intense than the even reflections due to the constant term in Eqn. 4.

In a first approximation the structure of the vacuum dried magnesium stearate bimolecular leaflet can be assumed to fit the same mathematical model as the barium stearate bimolecular leaflet because the unit cell dimensions D and the ratios of the intensities of odd and even orders of the first few reflections are very similar. There is evidence, however, that in magnesium stearate multilayers there are 2 separate layers of Mg^{2+} between two adjacent lipid hydrocarbon cores (see below). A Mg^{2+} then binds to two carboxyl groups of neighboring fatty acids in the same bimolecular leaflet. The structure of the hydrocarbon core, however, can be expected to be the same for both the barium and vacuum dried magnesium stearate bimolecular leaflet. It can be shown by trial and error that the only phase sequence which meets this criterion when the electron density distribution $\rho(x)$

$$\rho(x) = 2/D\cdot\sum_h |F(h)|\cdot\exp(-i\varphi_h)\cdot\exp(-2\pi i x h/D) \quad (5)$$

where

$$h^2\cdot I_{obs}(h) \propto |F(h)|^2$$

is calculated, is the sequence $\varphi_h = \pi,0,\pi,0,\pi,0,\pi,\pi,0$ for the orders $h = 1,2,\ldots.9$ (Fig. 2, top). The integrated intensities were corrected by a factor of h^2; one factor of h arises from the divergence of the X-ray beam[15], the other from the geometry of the specimen.

The characteristic electron density distribution of a fatty acid bimolecular-leaflet[13] can be seen in Fig. 2. The peaks of high electron density at the edges of the unit cell correspond to the regions of the Mg^{2+}. At the resolution to which $\rho(x)$ was calculated, the magnesium peaks do not separate from the edges of the unit cell, and the missing 8th peak is the only evidence that the layer of Mg^{2+} is not located

exactly at $\pm D/2$. The inner region of low electron density corresponds to the lipid hydrocarbon core composed of packed fatty acid chains. The trough in the center of the unit cell is the region of the terminal methyl groups of the fatty acid chains. The minima immediately inside of the magnesium peaks are due to truncation artefacts[13].

Fourier syntheses, $\rho(x)$, were calculated also for hydrated magnesium stearate, using intensity data for the specimen with 43 unit cells. It can be shown by trial and error that only one phase sequence for the first 6 reflections will result in a hydrocarbon core in $\rho(x)$ for the hydrated bimolecular leaflet, which is consistent with $\mu(x)$ obtained by deconvolution of $P_0(x)$. Furthermore, there is only one phase combination for the higher order reflections which results in a hydrocarbon core consistent with that for the vacuum dried structure and the barium stearate bimolecular leaflet. $\rho(x)$ calculated with this phase sequence $\varphi_h = \pi,0,\pi,0,\pi,\pi,0,\pi,0,\pi,0,\pi$ for the orders $h = 1,2 \ldots 12$ is shown in Fig. 2. The intensities were corrected by a factor of h^2 as in the vacuum dried case. This phase sequence places the peaks of high relative electron density slightly inside of $\pm D/2$. There is a region of low electron density between neighboring peaks of two adjacent bimolecular leaflets of approx. 3 Å width. D diminishes by approximately that amount when the structure is dehydrated. Since the only phase combination, which results in a hydrocarbon core of proper structure and dimension for a fatty acid bimolecular leaflet[13], is also the only one which results in a small region of low electron density between two bimolecular leaflets, which may be identified as water space, it may be considered to be the correct solution. The meaning of these phase sequences can be visualized on the basis of the model in Eqn. 3. The two symmetric δ-functions are now placed well inside of $\pm D/2$. Therefore, the maxima of the structure factor and the interference function[22] will get slowly but systematically out of phase. This occurs in the hydrated structure in the region of the 5th and 6th lamellar reflection and in the vacuum dried structure around the 8th reflection, because the alternating phase sequence for the model of Eqn. 3 is reversed in these regions of reciprocal space.

Magnesium stearate multilayers with incorporated ANS

The relative concentrations of ANS and stearic acid in the stock solution used to spread monomolecular films should be representative for the amount of ANS in the multilayer specimen. Although it cannot be excluded that some of the ANS disappears into the aqueous phase during the process of spreading in the Langmuir trough, most of the ANS must be contained in the multilayer specimen, since its fluorescence can be easily measured.

$P'(x)$ (Eqn. 2) can be calculated for the specimen with 3 unit cells of ANS/magnesium stearate (Fig. 3) as before with magnesium stearate. The electron density profile $\mu(x)$, obtained by deconvolution of $P_0(x)$, is shown in Fig. 4. It appears from Fig. 4 that at this resolution ANS causes only minor changes in the structure. This observation is consistent with the fact that at even higher ANS concentrations the basic structure of a phospholipid bimolecular leaflet is preserved. It can then be shown by trial and error, that only one phase combination for the first 6 reflections from the hydrated ANS/magnesium stearate specimen with 25 unit cells yields a $\rho(x)$ which is consistent with the respective $\mu(x)$ of Fig. 4, namely $\varphi_h = \pi,0,\pi,0,\pi,\pi$ for $h = 1,2,\ldots 6$. Similarly, there is only one phase combination for the first 6 reflections,

which results in a hydrocarbon core in $\rho(x)$ for the vacuum dried ANS/magnesium stearate specimen with 25 unit cells consistent with $\mu(x)$, namely $\varphi_h = \pi,0,\pi,0,\pi,0$ for $h = 1,2,\ldots 6$.

In order to find the phase angles for the reflections of order $h = 7,8$ and 9, the assumption is made that the form in $\rho(x)$ of the hydrocarbon core is similar for both the hydrated and vacuum dried specimens also in the case with incorporated ANS. The only phase combinations which meet this criterion are $\varphi_h = 0,\pi,0$ and $\varphi_h = \pi,0,\pi$ for $h = 7,8,9$ in the hydrated and vacuum dried structure, respectively. This is also the only phase sequence for the hydrated structure, which results in a small region of low electron density between adjacent bimolecular leaflets and allows, therefore, to account for the observed swelling behaviour. The reflection of order $h = 10$ of the hydrated structure is given the phase angle $\varphi_{10} = \pi$, because $\varphi_{10} = 0$ would result in a physically unreasonable structure for the center of the hydrocarbon core. The phase sequences for both hydrated and vacuum dried ANS/magnesium stearate thus are the same as for the respective structures without ANS, as might have been expected, because spacings and swelling behaviour of the respective structures are the same and the differences in the relative intensities, especially in the vacuum dried case, are not too large.

The electron density profiles $\rho(x)$ (Eqn. 5) are shown in Fig. 5. For comparison the electron density distributions of the pure magnesium stearate bimolecular leaflet were calculated to the same resolution and are included in Fig. 5. The absolute electron

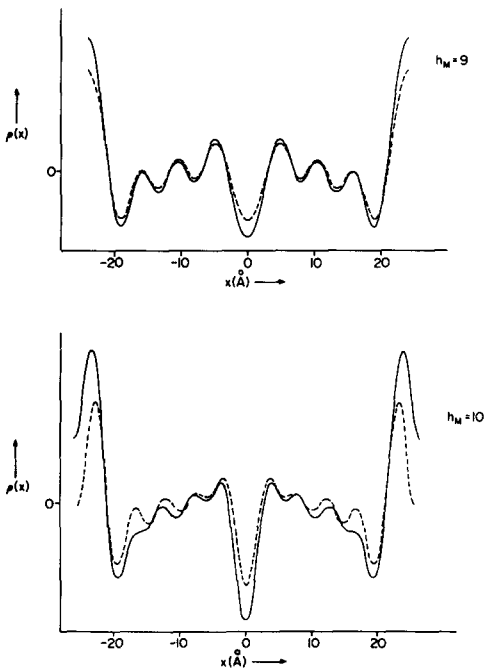

Fig. 5. Profile of the relative electron density $\rho(x)$ (in arbitrary units) of the magnesium stearate bimolecular leaflet with incorporated ANS (molar ratio stearate to ANS 5:1) in the vacuum dried (top) and the hydrated (bottom) state. h_M is the maximum number of reflections used in the Fourier synthesis. For comparison $\rho(x)$ of the respective magnesium stearate structure calculated to the same resolution is also given (– – – –). For normalization and scaling factors see text.

densities in $\mu(x)$ and $\rho(x)$ have not been determined. The average electron density of the total structure is chosen as the zero level in all cases. In Fig. 5 it was assumed that the average electron density is not changed in either hydrated or vacuum dried magnesium stearate, when ANS is incorporated in the structure and the zero levels have been superimposed. The Patterson functions have been normalized to 1.0 at the origin. This normalization implies a scaling of $\mu(x)$ and $\rho(x)$, since $\mu(x)$ is derived directly from $P_0(x)$ and since the intensities were corrected for calculating $\rho(x)$ in an analogous way as for the Patterson function.

Regardless of normalization and scaling factors, it appears from Fig. 5 that especially in the vacuum dried case and at the resolution obtained the general characteristics of the hydrocarbon cores, *viz.* methylene regions of nearly constant electron density separated by a well-defined methyl region, are the same for the structures with and without ANS. It is, therefore, physically reasonable to demand that the scaling procedure result in the same electron density for that region of the structures. The method of normalizing the intensities meets this criterion and, therefore no further scaling factors were applied. Only minor differences are to be expected for the vacuum dried structures with and without ANS on the basis of the differences and reproducibility of the diffracted intensities. The diffracted intensities for the hydrated structures with and without ANS, however, although following the same general pattern, are significantly different and this must correspond to differences in the two structures caused by ANS. $\rho(x)$ is the projection of the average electron density in the plane of the bimolecular leaflet onto the x-axis[16]. The differences in the hydrated structures then mean that incorporation of ANS results in the projection in a higher electron density of the polar regions, in a slightly lower density of the hydrocarbon core immediately inside the polar regions and in a deeper methyl trough. The fact that the water trough is filled up may be due in part to truncation error.

Phospholipid dispersions

Phospholipid dispersions prepared in the way outlined above are an aqueous suspension of small vesicles[10,11]. Their walls consist predominantly of single bimolecular leaflets[10,11]. Some vesicles may have a wall of two or more bimolecular leaflets, however, their mutual geometrical arrangement is not ordered enough to give rise to interference of coherently diffracted radiation or there are very few of them, because no discrete reflections can be seen in the diffraction pattern[21]. There is a wide distribution of diameters of the vesicles[17], if no special precautions are taken in the preparation[10,11]. The lower limit of the diameter lies at 250–350 Å. The vesicles have a near spherical shape as long as there is no osmotic gradient across the wall.

The essential prerequisite in order to apply the theories of HOSEMANN AND BAGCHI[14] and to obtain $P'(x)$, $P_0(x)$, and $\mu(x)$ is that diffraction data are obtained from systems with small enough numbers of coherently diffracting unit cells that the true width of the maxima of the interference function can be experimentally observed. Under these conditions $P'(x)$ is no longer a periodic function. Theoretically, $P'(x)$ has to disappear outside of $\pm N \cdot D$. The half-width of the reflections determine this behaviour and it was shown for the barium stearate[13] and the magnesium stearate bimolecular leaflet (see above) that experimental $P'(x)$ rapidly disappears outside $\pm N \cdot D$ and that N can be determined from $P'(x)$ for at least $N < 4$. $P'(x)$ for the lecithin/cardiolipin dispersion is shown in Fig. 6. It appears from Fig. 6 that $P'(x)$

has very small values outside of approx. ± 50 Å. The thickness of the phospholipid bimolecular leaflet is approx. 50 Å, and the diffracted intensity from the dispersion must arise, therefore, from single bimolecular leaflets at least with regard to the half-width and shape of the diffraction maxima. In other words, $P_0(x)$ is identical with $P'(x)$ (see Fig. 6; dots in Fig. 6 correspond to calculated $P_0(x)$). (For a dispersion D is defined as the distance between the points where the electron density differs for the first time from the average electron density of the total system when approaching the bimolecular leaflet from the water space along $\pm x$.)

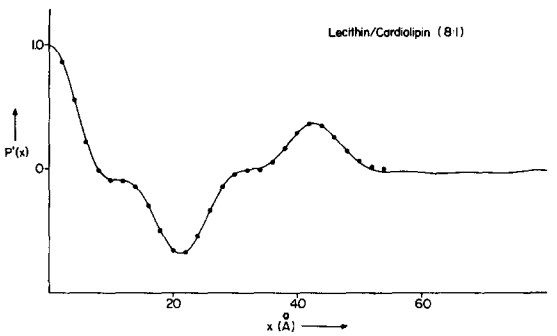

Fig. 6. Generalized Patterson function $P'(x)$ for a single dipalmitoyllecithin/cardiolipin bimolecular leaflet, as obtained by an integral Fourier transformation of $I_{obs}(x^*)$ from the phospholipid dispersion. Normalization is for $P'(0) = 1.0$. Dots refer to computed $P_0(x)$.

Furthermore, a comparison of discrete reflections from phospholipid multilayers with the intensity function from dispersions[18] shows that the relative integrated intensities from the multilayer specimens at high relative humidity, placed at the appropriate coordinates $x^* = h/D$, match the continuous intensity function from the dispersion in the observed region of x^*. The diffracted intensities from the dispersion, therefore, are proportional to the spherically averaged absolute square of the Fourier transform of the electron density distribution of the bimolecular leaflet, taking proper correction factors into account (see APPENDIX).

The electron density profile $\mu(x)$ can then be obtained by deconvoluting $P_0(x)$ (Fig. 8). The proper x-coordinate from which the deconvolution is to be started must be determined by trial and error, since the experimentally determined generalized Patterson function does not exactly disappear outside $\pm D$ due to truncation artefacts. The best methods to determine the proper value of D were found to be a search for that D which satisfies $P_0(x) = P'(x)$ or which results in a symmetric $\mu(x)$. The correct μ-function can be selected, because the solution has to be symmetric and the symmetric solution is unique[14]. Best results were obtained with $D = 54.0$ Å. $\mu(x)$ shows two peaks of high electron density at ± 22–23 Å separated by a region of low electron density.

These regions are ascribed to the layer of the polar groups of the phospholipids and the lipid hydrocarbon core, respectively. The trough at $x = 0$ corresponds to the region of the terminal methyl groups of the fatty acid chains. The electron density of that region, as in the fatty acid multilayers, is expected to be lower than in the region of the methylene groups[19]. The larger width of the methyl trough compared to the fatty acid bimolecular leaflet may be explained by differences in chain length

of the fatty acids of the phospholipids used. If the fatty acids have small differences in chain length, the packing density in the center of the hydrocarbon core may be decreased to a greater extent than by the terminal methyl groups alone. The slight asymmetry in the μ-function is due to computation artefacts[13], mainly arising from the choice of finite intervals Δx and Δx^* for the sampling of $P_0(x)$ (see APPENDIX) and the intensity data.

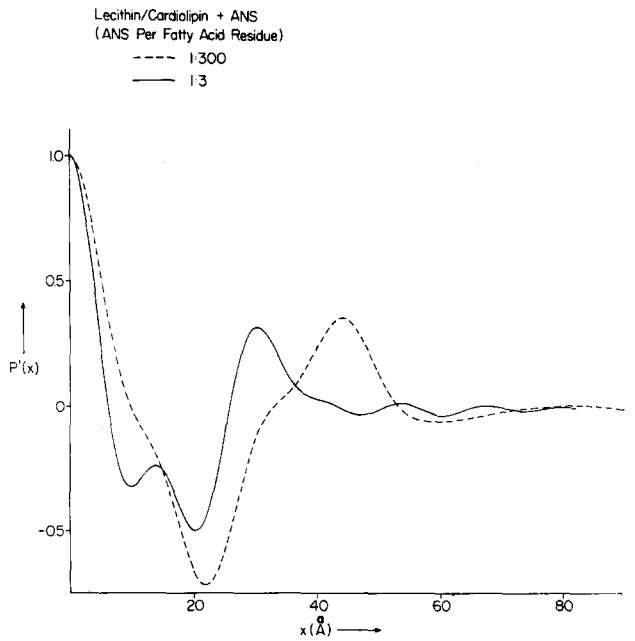

Fig. 7. Generalized Patterson function $P'(x)$ for the dipalmitoyllecithin/cardiolipin bimolecular leaflet with incorporated ANS. ANS concentrations are 1 ANS molecule per 3 (———) and per 300 (– – – –) fatty acid residues of the phospholipids. Normalization is for $P'(0) = 1.0$.

$P'(x)$ and $\mu(x)$ for lecithin/cardiolipin with incorporated ANS is shown in Figs. 7 and 8, respectively. The thickness of the bimolecular leaflet is not affected, if ANS is incorporated in the lecithin/cardiolipin bimolecular leaflet in the low concentration of one ANS molecule per 300 fatty acid residues ($D = 54.0$ Å). The central trough in the electron density distribution has become wider and the peaks of high electron density in the region of the polar groups extend further into the interior of the unit cell than in the reference structure. This means that both the structure of the layer of the polar groups and of the hydrocarbon core are perturbed.

A marked decrease in D occurs if ANS is present in the higher concentration of one ANS molecule per 3 fatty acid residues (Figs. 7, 8). The best value for D is 39.0 Å. The electron density function shows that even at such high ANS concentrations the general structure of the bimolecular leaflet is preserved. The region of the polar groups is of comparable width to the reference and the decrease in D is due to a decrease in the thickness of the lipid hydrocarbon core. The resolution of the μ-function is determined by that of the Patterson function from which it is derived. The small peak in the center of the hydrocarbon core is not likely to be significant.

The average electron density of the whole hydrocarbon core is lower than in the reference and a well-defined methyl region is absent. No such collapse of the hydrocarbon core was observed in the magnesium stearate bimolecular leaflet. One reason for this may be that the ANS concentration there was not as high as here. Regardless of ANS, however, the hydrocarbon cores of the fatty acid and phospholipid bimolecular leaflets differ with regard to the unsaturation and homogeneity of the fatty acid composition. The glyceryl phosphoryl choline residues of the phospholipids may also affect the structure of the hydrocarbon interior.

Electron density distributions for dispersions can be calculated also by a Fourier transformation of the square root of the intensity function in order to study the internal consistency of the deconvolution procedure. Values for the phase angle in

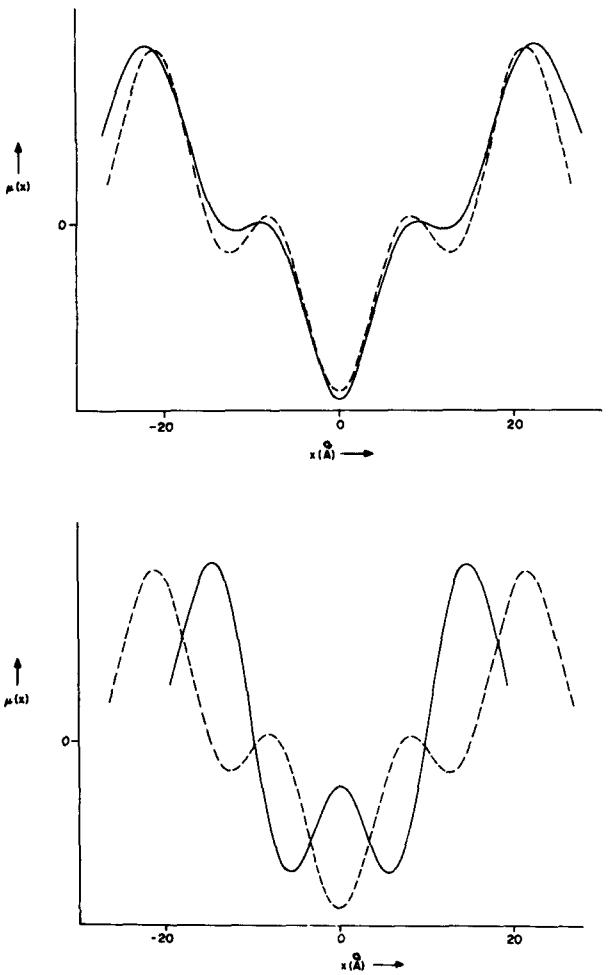

Fig. 8. Profile of the relative electron density $\mu(x)$ (in arbitrary units) for the dipalmitoyllecithin/cardiolipin bimolecular leaflet with incorporated ANS in low (top) and high (bottom) concentration. ANS concentrations are 1 ANS molecule per 3 and 300 fatty acid residues of the phospholipids. As reference, $\mu(x)$ for the dipalmitoyllecithin/cardiolipin bimolecular leaflet without ANS is included (-----).

the intervals of the reciprocal space coordinate within each of the maxima of the intensity function must then be chosen. It may be noted that for each dispersion pattern, one and only one of the several possible electron density functions obtained by such a Fourier synthesis was identical with the corresponding μ-function whereas all the other Fourier syntheses were not even similar to $\mu(x)$. The combination of phase angles for this to occur was $\pi, 0, \pi$ for the 3 maxima in the intensity function for the dispersions of lecithin/cardiolipin and lecithin/cardiolipin with low ANS content. For the lecithin/cardiolipin dispersion with the high ANS concentration the μ-function was reproduced by a Fourier synthesis with phase angles of π and 0 for the first and second maximum.

CONCLUSIONS

The number of coherently diffracting unit cells in the lipid model systems used in these experiments can be controlled in several ways. It was shown by HOSEMANN AND BAGCHI[14] that a direct analysis of X-ray diffraction can be performed if intensity data are obtained from systems with a small enough number of unit cells that the true width of the maxima of the interference function can be observed experimentally. The autocorrelation function $P_0(x)$ can then be calculated from a generalized Patterson function $P'(x)$, obtained by an integral Fourier transformation of the observed intensity function.

Experimentally determined $P'(x)$ disappears rapidly outside $\pm N \cdot D$, and N can be determined from $P'(x)$. $P'(x)$ was calculated for a system with 3 unit cells of magnesium stearate. The electron density distributions $\mu(x)$ of these systems can be derived by deconvoluting $P_0(x)$, since they are centrosymmetric. $\mu(x)$ for hydrated magnesium stearate shows peaks of high relative electron density near $\pm D/2$ (Mg^{2+}) and an inner hydrocarbon core with low and nearly constant electron density (methylene region) with a central trough (methyl region of the fatty acid chains).

$\mu(x)$ determines the phase angles of the first 6 lamellar reflections from hydrated structure with a large number of unit cells. The phase angles of the observed higher order reflections of the many unit cell structures are determined by swelling experiments and comparison with the barium stearate structure whose electron density profile has been established previously to much higher resolution[13].

A similar phasing argument is developed for magnesium stearate with incorporated ANS. Fourier syntheses $\rho(x)$ are calculated with the thus established phase sequences. All $\mu(x)$ and $\rho(x)$ show that the basic structure of the magnesium stearate bimolecular leaflet, as revealed by the projection of the electron density in the plane of the leaflet onto the x-axis, is preserved when ANS is added. With a molar stearate: ANS ratio of 5:1, the sulfonate group of ANS would have to be resolved, if the ANS molecules were completely buried in the hydrocarbon core, as can be verified by model calculations.

These findings are consistent with a model in which the sulfonate group of the ANS molecule is located in the layer of the magnesium ions, and the apolar residue of ANS, probably the naphthalene ring, penetrates in between the fatty acid chains of the bimolecular leaflet. The higher electron density in the layer of magnesium ions and the slightly perturbed structure of the hydrocarbon core immediately inside the magnesium peak in the hydrated ANS/magnesium stearate structure support this model.

Phospholipid dispersions may be regarded with good approximation as a system of randomly oriented planes of single bimolecular leaflets. $\mu(x)$ of the phospholipid bimolecular leaflet shows two peaks of high relative electron density separated by a region of low electron density and a central trough; these regions are ascribed to the layer of polar groups (mainly phosphorus atoms), and to the methylene and methyl regions, respectively[19]. ANS in low concentrations has minor effects on the structure at the resolution obtained. At high ANS concentration, however, the thickness of the bimolecular leaflet decreases by approx. 15 Å. This is mainly due to a perturbation of the structure of the hydrocarbon core. A model analogous to that derived for the magnesium stearate structure can be discussed for the location of ANS in the phospholipid bimolecular leaflet. The sulfonate group of ANS with its relatively high electron density has to be placed in the layer of the polar groups of the phospholipids. The most probable reason for the decrease in D at high ANS concentrations is that at least a part of the apolar residue, probably the naphthalene ring, penetrates in between the fatty acid chains of the hydrocarbon core. This apolar residue is much shorter than the average fatty acid chain. It is well known that mixed crystals of fatty acids of different chain length show long spacings in X-ray diffraction patterns which lie between the values observed with the pure components[20]. The analogous phenomenon should occur in phospholipid bimolecular leaflets with a high content of ANS, if it is located as discussed in the above model.

Fluorescent molecules like ANS are used as probes for the structure of biological membranes. It is well known that ANS binds to apolar regions of protein molecules[1]. However, if an aggregation of polar lipid molecules into a lipid hydrocarbon core is part of the structure of a biological membrane, ANS will be incorporated also in that part of the membrane. In higher concentrations ANS can change the molecular architecture of such regions. These observations may help to explain the complexity of the fluorescence response of ANS when bound to biological membranes.

APPENDIX I

Derivation of the autocorrelation function $P_0(x)$

The one-dimensional generalized Patterson function $P'(x)$ (Eqn. 2) can be written

$$P'(x) = 1/D \cdot \{P_0(x) * [l(x) \cdot \sigma(x)]\}; \qquad \sigma(x) = s(x) * s(-x)$$

($l(x)$ = one-dimensional lattice function; $s(x)$ = shape function, defined as $s(x) = 1$ and $s(x) = 0$ for $|x| \leqslant N \cdot D$ and $|x| > N \cdot D$, respectively. $P'(x)$ can be represented, therefore, by a convolution of $P_0(x)$ with a weighted lattice function $[l(x) \cdot \sigma(x)]$, where $[l(x) \cdot \sigma(x)]_{x = j \cdot D} = P'(j \cdot D)/P_0(0)$, with $j = 0, 1, \ldots N$.

The following equations can then be derived

$$P'(x_i) = \{P'(0) \cdot P_0(x_i) + P'(D) \cdot P_0(x_i - D)\}/P_0(0)$$

$$P'(x_i - D) = \{P'(0) \cdot P_0(x_i - D) + P'(D) \cdot P_0(x_i)\}/P_0(0)$$

and can be solved for $P_0(x_i)$ for any x_i in $0 \leqslant x_i \leqslant D$(ref. 13). Two new functions $p(x)$ and $\mu(x)$ are defined after HOSEMANN AND BAGCHI (ref. 14, p. 123).

$$p(x) = \int_{x-\Delta x/2}^{x+\Delta x/2} P_0(u)\, du; \qquad \mu(x) = \int_{x-\Delta x/2}^{x+\Delta x/2} \rho(u)\, du$$

$\mu(x)$ can be obtained by deconvoluting $p(x)$ by a recursion formula, since in the one-dimensional case

$$p(-D + h\cdot\Delta x) = \sum_{i=0}^{h} \mu(i\cdot\Delta x)\cdot\mu([h-i]\cdot\Delta x); \qquad h = 0,1,2,\ldots D/\Delta x \tag{3}$$

APPENDIX II

Intensity correction factors for phospholipid dispersions

A phospholipid vesicle may be treated as a spherical shell of average radius R_0, whose wall is a bimolecular leaflet. The spherically symmetric electron density distribution is $\rho(r)$. Its Fourier transform $G(\vec{r^*})$ is

$$G(r^*) = 2\pi \int_0^{\infty} r^2\cdot\rho(r)\cdot\sin(2\pi r r^*)/\pi r r^* \, \mathrm{d}r$$

The bimolecular leaflet extends from $r = R-D/2$ to $r = R+D/2$ and is assumed to be symmetric around R. A symmetric function can be described approximately by a set of narrowly spaced and pairwise symmetric δ-functions.

$$\rho(r) = \sum_{i=0}^{h} A(u_i)\cdot\{\delta(r-[R+u_i]) + \delta(r-[R-u_i])\}; \qquad u_i = i\,\Delta r; \qquad n = D/2\cdot\Delta r$$

where $A(u)$ is a scaling function. Then

$$|G(r^*)|^2 \propto \text{const.} \sum_{i=0}^{h} A^2(u_i)/(r^*)^2\cdot\{R^2\cdot\sin^2(2\pi r^* R)\cdot\cos^2(2\pi r^* u_i) +$$
$$u_i/2\cdot R\cdot\sin(4\pi r^* R)\cdot\sin(4\pi r^*\cdot u_i) + u_i^2\cdot\cos^2(2\pi r^* R)\cdot\sin^2(2\pi r^* u_i)\}$$

R_0 is the average radius of the vesicles. If a gaussian distribution $M(R)$ of the values of R is assumed,

$$M(R) = \exp(-\beta[R-R_0]^2)$$

the coefficients of the first, second and third term in $|G(\vec{r})^*|^2$ have to be replaced by

$$c\cdot\int_0^{\infty} R^2\cdot M(R)\cdot\sin^2(2\pi r^* R)\,\mathrm{d}R, \qquad c\cdot u_i/2\cdot\int_0^{\infty} R\cdot M(R)\cdot\sin(4\pi r^* R)\,\mathrm{d}R$$

and

$$c\cdot u_i^2\cdot\int_0^{\infty} M(R)\cdot\cos^2(2\pi r^* R)\,\mathrm{d}R,$$

respectively, where

$$c = 1\Big/\int_0^{\infty} M(R)\,\mathrm{d}R.$$

These integrals can be solved and it can be shown that the second and third term in $|G(\vec{r^*})|^2$ can be neglected with good approximation:

$$|G(r^*)|^2 \sim \sum_{i=0}^{h} A^2(u_i)\cdot\frac{\cos^2(2\pi r^* u_i)}{(r^*)^2}$$

The errors $\varepsilon(R,r^*,u_i)$ introduced by this approximation are of the order of less than $D^2/4 \cdot R_0^2$, since $u_i \leqslant D/2$ and since intensity data were recorded for $r^* > 1/R_0$ only. With values for $D \sim 50$ Å and $R_0 \sim 150$ Å, these errors already are less than 3 % of $|G(r^*)|^2$. Dispersions may, therefore, be treated as a system of randomly oriented planes of single bimolecular leaflets.

ACKNOWLEDGEMENTS

The authors thank Dr. C. P. Lee for the gift of purified ANS. This work was supported by the U.S. Public Health Service grant G.M. 12202.

REFERENCES

1 L. STRYER, *J. Mol. Biol.*, 13 (1965) 482.
G. WEBER, *Biochem. J.*, 51 (1952) 155.
2 A. AZZI, B. CHANCE, G. K. RADDA AND C. P. LEE, *Proc. Natl. Acad. Sci. U.S.*, 62 (1969) 612.
3 L. ERNSTER AND K. NORDENBRAND, *Biochem. J.*, 116 (1969) 13P.
4 J. R. BROCKLEHURST, R. B. FREEDMAN, D. J. HANCOCK AND G. K. RADDA, *Biochem. J.*, 116 (1970) 721.
5 T. GULIK-KRZYWICKI, E. SHECHTER, M. IWATSUBO, J. L. RANK AND V. LUZZATI, *Biochim. Biophys. Acta*, 219 (1970) 1.
6 W. LESSLAUER AND J. K. BLASIE, *1st Discuss. Conf. Macromol., Models Biopolym. Struct. Funct., Mariánské Lázně, 1970.*
7 G. WEBER AND L. B. YOUNG, *J. Biol. Chem.*, 239 (1964) 1415.
8 K. B. BLODGETT, *J. Am. Chem. Soc.*, 57 (1935) 1007.
9 I. H. SHER AND J. C. CHANLEY, *Rev. Sci. Instrum.*, 26 (1955) 266.
10 A. D. BANGHAM, M. M. STANDISH AND J. C. WATKINS, *J. Mol. Biol.*, 13 (1965) 238.
11 C. HUANG, *Biochemistry*, 8 (1969) 344.
12 G. F. ELLIOTT AND C. R. WORTHINGTON, *J. Ultrastruct. Res.*, 9 (1963) 166.
13 W. LESSLAUER AND J. K. BLASIE, *Biophys. J.*, in the press.
14 R. HOSEMANN AND S. U. BAGCHI, *Direct Analysis of Diffraction by Matter*, North Holland Publ. Co., Amsterdam, 1962.
15 A. E. BLAUROCK AND C. R. WORTHINGTON, *Biophys. J.*, 6 (1966) 305.
16 W. LESSLAUER AND J. K. BLASIE, *Acta Crystallogr.*, in the press.
17 V. K. MIYAMOTO, G. W. POHL AND W. STOECKENIUS, *Biophys. J.*, 9 (1969) A-175.
18 W. LESSLAUER, J. CAIN AND J. K. BLASIE, *Biophys. Soc. Abstr., Biophys. J.*, 11 (1971) 13A.
19 Y. K. LEVINE, O. I. BAILEY AND M. H. F. WILKINS, *Nature*, 220 (1968) 577.
20 D. G. DERVICHIAN, *The Physical Chemistry of Phospholipids*, in *Progr. Biophys. Mol. Biol.*, 14 (1964) 284.
21 Reported in J. O. LUCY, *FEBS Letters*, 3 (1969) 297.
22 R. W. JAMES, *The Optical Principles of the Diffraction of X-rays*, Cornell Univ. Press, Ithaca, 1965.